Electrochemical and Microbiological Response of Exoelectrogenic Biofilm to Polyethylene Microplastics in Water

Wang, Song; Xu, Mingyi; Jin, Biao; Wünsch, Urban; Su, Yanyan; Zhang, Yifeng

Published in:
Water Research

Link to article, DOI:
10.1016/j.watres.2022.118046

Publication date:
2022

Document Version
Peer reviewed version

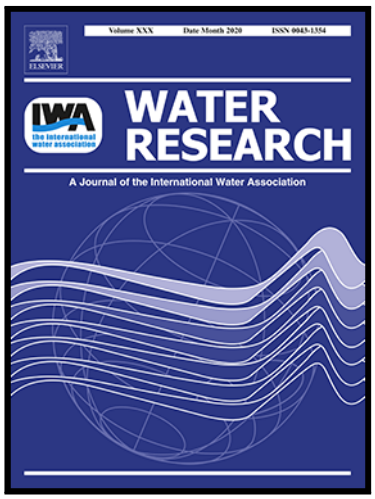

Electrochemical and Microbiological Response of Exoelectrogenic Biofilm to Polyethylene Microplastics in Water

Song Wang , Mingyi Xu , Biao Jin , Urban Wünsch , Yanyan Su , Yifeng Zhang

PII: S0043-1354(22)00009-4
DOI: https://doi.org/10.1016/j.watres.2022.118046
Reference: WR 118046

To appear in: *Water Research*

Received date: 26 October 2021
Revised date: 25 December 2021
Accepted date: 5 January 2022

Please cite this article as: Song Wang , Mingyi Xu , Biao Jin , Urban Wünsch , Yanyan Su , Yifeng Zhang , Electrochemical and Microbiological Response of Exoelectrogenic Biofilm to Polyethylene Microplastics in Water, *Water Research* (2022), doi: https://doi.org/10.1016/j.watres.2022.118046

Electrochemical and Microbiological Response of Exoelectrogenic Biofilm to Polyethylene Microplastics in Water

Song Wang[a], Mingyi Xu[a], Biao Jin[b], Urban Wünsch[c], Yanyan Su[d,*], Yifeng Zhang[a,*]

a Department of Environmental Engineering, Technical University of Denmark, DK-2800 Lyngby, Denmark

b State Key Laboratory of Organic Geochemistry, Guangzhou Institute of Geochemistry, Chinese Academy of Sciences, Guangzhou 510640, China

c National Institute of Aquatic Resources, Section for Oceans and Arctic, Technical University of Denmark, Kemitorvet, Kgs. Lyngby 2800, Denmark

d Carlsberg Research Laboratory, Bjerregaardsvej 5, 2500 Valby, Denmark

[*] Corresponding authors: yifz@env.dtu.dk, yifzmfc@gmail.com (Yifeng Zhang); yanyansu@daad-alumni.de (Yanyan Su). Tel.: +45 45251410; fax: ++45 45932850.

Highlights

First study of the response of exoelectrogenic biofilm to microplastics.
Polyethylene microplastics declined current density of microbial electrolysis cell.
Polyethylene microplastics inhibit the cell viability, increased dead cell ratio.
Extracellular polymeric substances declined with the occurrence of microplastics.
Extracellular electron transfer related genes and cytochrome c decreased.

Graphic. Abstract

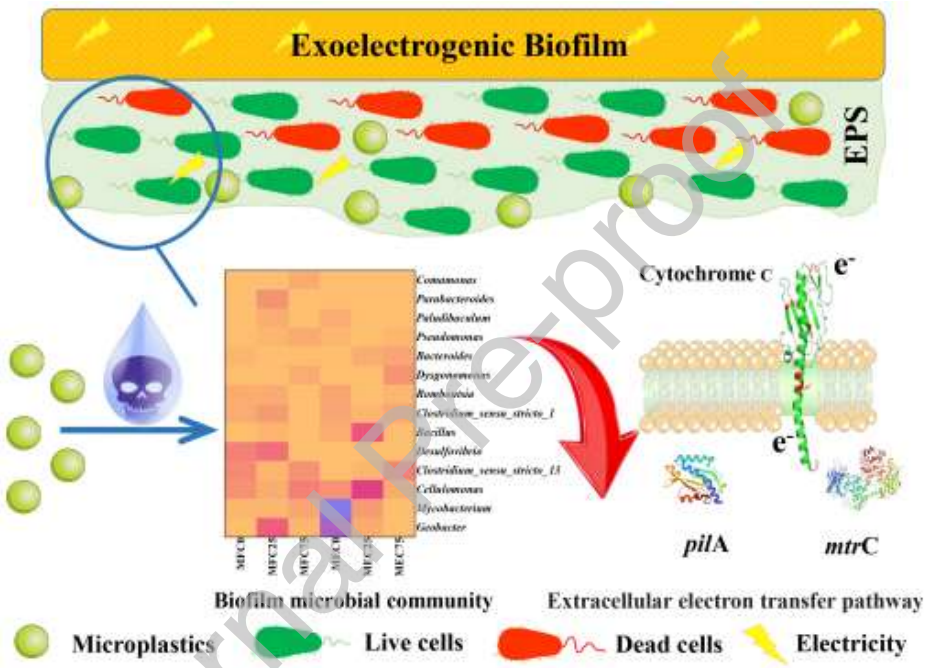

Abstract

Exoelectrogenic biofilm and the associated microbial electrochemical processes have recently been intensively studied for water treatment, but their response to and interaction with polyethylene (PE) microplastics which are widespread in various aquatic environments has never been reported. Here, we investigated how and to what extent PE microplastics would affect the electrochemistry and microbiology of

exoelectrogenic biofilm in both microbial fuel cells (MFCs) and microbial electrolysis cells (MECs). When the PE microplastics concentration was increased from 0 to 75 mg/L in the MECs, an apparent decline in the maximum current density (from 1.99 to 0.74 A/m^2) and abundance of electroactive bacteria (EAB) in the exoelectrogenic biofilm was noticed. While in the MFCs, the current output was not significantly influenced and the abundance of EAB lightly increased at 25 mg/L microplastics. In addition, PE microplastics restrained the viability of the exoelectrogenic biofilms in both systems, leading to a higher system electrode resistance. Moreover, the microbial community richness and the microplastics-related operational taxonomic units decreased with PE microplastics. Furthermore, the electron transfer-related genes (e.g., *pil*A and *mtr*C) and cytochrome c concentration decreased after adding microplastics. This study provides the first glimpse into the influence of PE microplastics on the exoelectrogenic biofilm with the potential mechanisms revealed at the gene level, laying a methodological foundation for the future development of efficient water treatment technologies.

Keywords: microplastics; microbial exoelectrogenic biofilm; microbial electrochemical systems; extracellular electron transfer

1. Introduction

Microplastics (MPs), plastic particles less than 5 mm, have been found worldwide, prevalent in the terrestrial and aquatic environment (wastewater, rivers, lakes, and ocean) and even in the secluded environment (Peeken et al., 2018; Rochman, 2018; Woodward et al., 2021). The amount of MPs in the environment is growing fast due to the degradation of plastics from industrial abrasives and personal care products, especially during the COVID-19 period when the face masks are extensively consumed (Kwak and An, 2021; Sun et al., 2020). The vast majority of microplastics from domestic and industrial wastewater would flow into the wastewater treatment systems (Zhang et al., 2020a). The MPs concentration found in the influent of Danish municipal sewage treatment plants was as high as 29.6 mg/L (Vollertsen and Hansen, 2017). In the influent of a wastewater treatment plant in South Korea, it could reach 31400 particles/L (Hidayaturrahman and Lee, 2019). Furthermore, high concentration of nano-polystyrene and polyethylene microplasitics (e.g., 320 mg/L and 100 mg/L, respectively) were used to reveal the influence on cell viability and wastewater biotreatment performance (Sun et al., 2018; Tang et al., 2021). With the continued use of the plastic product, the concentration of microplastics would accumulate to a considerable concentration because of the hard-degradable properties.

MPs are considered an emerging threat because they are important vectors of different pollutants, including antibiotics, heavy metals, and micropollutants (Avio et al., 2017; Niu et al., 2021; Sarkar et al., 2021). It has been estimated that the MPs in the body of organisms could induce a physical toxicity disturbance and digestive system entanglements resulting in the damage of aquatic ecosystems (Niu et al., 2021; Seidensticker et al., 2017). Nano polystyrene plastics could easily enter the body of

organisms such as invertebrates (Cole and Galloway, 2015; Trevisan et al., 2019), and plants (Sun et al., 2020) and trigger severe adverse responses. Besides, evidence also showed that MPs could influence microbial activities and metabolisms by reshaping their community structure. For example, polyethylene terephthalate MPs could inhibit the hydrolysis process in aerobic digestion (Wei et al., 2021). The methanogenesis process could be significantly restrained by long-term exposure to polyvinyl chloride MPs because of the alteration of microbial composition (Zhang et al., 2020a). It was also reported that the microbial nitrogen cycle in the sediment could be interfered with by different kinds of MPs (Seeley et al., 2020). The capacity of wastewater treatment could be influenced in the presence of MPs (Qin et al., 2020; Zhang et al., 2020b). However, the study of MPs and their effect on natural or engineered processes is in its infancy. A deeper understanding of the role of MPs in several key microbial processes is still missing.

Microbial electrochemical systems (MESs) such as microbial fuel cells (MFCs) and microbial electrolysis cells (MECs), which employ electroactive bacteria (EAB) to harvest electrons from organic or inorganic pollutants, have been widely studied and considered a promising and energy-efficient approach for wastewater treatment and clean production of high-value chemicals (Chiranjeevi and Patil, 2020; Wang and Ren, 2013; Bajracharya et al., 2016; Fu et al., 2021). The activity of EAB and the formed biofilm is the crucial element that determines the extracellular electron transfer (EET) ability and the electrogenesis performance of various MESs. Extracellular polymeric substances (EPS) are fundamental components and complex chemical microenvironments in the structure of biofilm. They could prevent the biofilm from being attacked by antibiotics and immune cells, playing essential roles in the microbial EET process (Karygianni et al., 2020; Xiao and Zhao, 2017). Besides,

cytochrome c and nicotinamide adenine dinucleotide (NADH) play critical roles in microbial extracellular and intracellular electron transfer processes (Xiao and Zhao, 2017; Zhang et al., 2021b). Several studies have shown that the EPS and microbial composition on the EAB biofilm could be influenced and even reshaped due to substrate limitation and the exposure of different toxicants (Hou et al., 2020; Li et al., 2021). It has been reported that nanoparticles (silver) can affect the microbial composition of anodic biofilm, EPS composition, and EET-associated genes (Zakaria and Dhar, 2020). As wastewater nowadays may contain a substantial amount of MPs, it could probably influence the electrochemical activity and microbiology of EAB biofilm in the process of wastewater treatment, which has never been reported.

In this study, for the first time, the impact of polyethylene MPs (PE-MP) on the exoelectrogenic biofilm and the associated extracellular electron transfer processes and the underlying mechanisms were explored. The response of the electrogenesis biofilm to MPs was investigated in terms of electrochemical characteristics, biofilm morphology, EPS composition, and microbial community structure. Lastly, the variation of EAB abundance, EET-associated genes, and protein was analyzed. This study may shed light on the evolution of electroactive bacteria and biofilm and resilience of the associated engineered processes/systems under specific environmental stress.

2. Methods and materials

2.1. Sources of inoculum and PE-MP.

Wastewater from Lundtofte municipal wastewater treatment plant (Lyngby, Denmark) was used as the inoculum in the MESs. The chemical oxygen demand (COD), total solids (TS), ammonium nitrogen from the wastewater were 300, 3.53, and 2.12 mg/L, respectively. Polyethylene is one of the most ubiquitous polymers in

111 water bodies (Cook et al., 2020). PE-MP (Cat no.434272. Sigma-Aldrich) with the
112 particle size range of 40-48 μm were used.

113 **2.2. Reactor configuration and operation.**

114 Twelve cuboid double chamber MES reactors were designed as previously
115 described (Yang et al., 2021). The anode (5×5×8 cm^3) and cathode (5×5×8 cm^3)
116 chamber were separated by a cation exchange membrane (CMI 70001, Membrane
117 international, NJ). The membrane was immersed in a 5% NaCl solution for 12 hours
118 to allow for membrane hydration and expansion. This preconditioning procedure can
119 also improve the diffusion permeability (Berezina et al., 2008; Xu et al., 2021) A
120 carbon fiber brush (diameter 5.0 cm, length 5.0 cm, Mill-Rose, USA, pretreated at
121 450 ^oC for 30 min) was used as anode and a titanium woven wire mesh (4.5 ×4.5 cm)
122 was used as cathode. Cathode was coated with 0.5 mg/cm^2 platinum to keep a stable
123 cathode reduction rate (Luo et al., 2014). Titanium wire was used to connect the
124 anode and cathode through an external resistance for operation in MFCs (1000 Ω) and
125 MECs (10 Ω) modes.

126 The multiple reactors were divided into six duplicate groups by different
127 operation modes (MFCs/MECs) and different PE-MP concentrations (0, 25, 75 mg/L),
128 marked as MFC0, MFC25, MFC75, MEC0, MEC25, and MEC75. During the setup
129 process, the anode of both MFCs and MECs were filled with wastewater together with
130 1 g/L sodium acetate and 50 mM phosphate buffer solution (PBS). The catholyte of
131 MFCs was a solution containing 50 mM PBS and 50 mM ferricyanide. As for MECs,
132 only 50 mM PBS was used in the cathode. All reactors were operated in a batch mode
133 at room temperature, and the medium in both chambers was refreshed every seven
134 days. After refreshing the anolyte, the anode of all reactors was flushed with nitrogen
135 gas for 15 min to keep an anaerobic atmosphere. The anolyte was continuously stirred

at 200 rpm during the batch. An external voltage of 0.8 V was applied to the groups in MEC mode.

2.3. Analytical methods.

2.3.1. Physico-chemical analysis and calculation.

COD was measured using the APHA standard method (Association et al., 2017). The voltage through the external resistance of all reactors was recorded using a multimeter (Model 2700, Keithley Instruments, Inc., Cleveland, OH, USA) with a 30-min interval. The current was calculated using Ohms Law (I=V/R). Power density (P = IV/A) was calculated based on the projected surface of the cathode (Zhao et al., 2019).

2.3.2. Electrochemical analysis.

Cyclic voltammetry (CV) and electrochemical impedance spectroscopy (EIS) analysis were conducted by using a potentiostat (Ivium-n-Stat, Ivium Technologies, Eindhoven, the Netherlands) with three-electrode configuration (i.e., anode as the working electrode, Ag/AgCl as a reference electrode, and cathode as the counter electrode). CV was performed from -0.8 to +0.8 V at a scanning rate of 2.5 mV/s. EIS was carried out from 10,000 to 0.1Hz with an amplitude of 10 mV. Resistance data including ohmic resistance (Rs), charge transfer resistance (Rct), and finite diffusion resistance (Rd) were calculated after fitting the Nyqusit plots with equivalent circuit model according to previous methods (Wang et al., 2020a).

2.3.3. The extraction and analysis of EPS.

A heating method was used to extract different EPS fractions from the anode biofilm at the end of the experiment (Li et al., 2021). The carbon brush with biofilm was rinsed in 0.9% NaCl and then heated at 70 ^{o}C for 30 minutes, followed by centrifuging at 10750 g for 15 minutes. The suspension was collected and filtered

161 through a 0.22 μm filter as loosely bound EPS (LB_EPS). The carbon brush left in the
162 centrifuge tube was then resuspended in 0.9% NaCl and 5% Na_2-EDTA, then shaken
163 at 180 rpm for 4 h. The collected suspension was filtered and obtained as tightly
164 bound EPS (TB_EPS). The EPS obtained above were characterized with excitation-
165 emission matrix (EEM) fluorescence spectroscopy. EEMs were measured using an
166 AquaLog fluorometer (HORIBA) to show the changes of LB_EPS and TB_EPS.
167 Absorbance and fluorescence excitation was measured from 240 to 600 nm in 3 nm
168 increments. Fluorescence emission was recorded with a charge-coupled device from
169 220 to 620 nm at an increment of approximately 3.3 nm at integration times of 1-3
170 seconds. Samples with absorbance exceeding 1.5 cm^{-1} were diluted before
171 measurements. Data were processed in MATLAB (The MathWorks Inc.) using the
172 drEEM toolbox (v0.6.3) as follows (Murphy et al., 2013). Raw data were imported
173 and blanks subtracted from the sample fluorescence. Inner filter effects were corrected
174 with the absorbance-based method (Kothawala et al., 2013). Fluorescence signals
175 were normalized to the Raman peak area at excitation 350 nm. First and second-order
176 Rayleigh and Raman scatter were excised and interpolated excised (1^{st} and 2^{nd} order
177 scatter) and interpolated (only 2^{nd} order scatter). Fluorescence intensities were
178 extracted at predefined wavelength pairs according to established procedures (Coble,
179 2007).

180 *2.3.4. Biofilm Viability Observations*.

181 Live/Dead cells were visualized to evaluate the viability of biofilm on the surface
182 of the anodic carbon brush under different PE-MP concentrations. The carbon brush
183 samples were collected in triplicate for each reactor at the end of the experiment. The
184 viability of the biofilm on the carbon brush was observed using the Confocal Laser
185 Scanning Microscopy (CLSM) (Leica TCS SP5, Germany). Before the observations,

the biofilm samples were rinsed with 50 mM PBS, then stained with a LIVE/DEAD BacLight bacterial viability kit (Invitrogen, Carlsbad, CA, United States) and incubated in the dark for 15 min, and afterward rinsed with 50 mM PBS twice to remove the residual fluorochrome. The biofilm was measured under the z-stack mode. The green and red dyes of SYTO-9 and propidium iodide were used to stain the live and dead cells, which could emit green and dead fluorescence, respectively. The excitation and emission for SYTO-9 are 488 nm and 500-550 nm, for propidium iodide are 561 nm and 570-650 nm. The mean fluorescence intensity was calculated from the triplicate samples based on the corresponding CLSM data. The three-dimensional biofilm was reconstructed using Imaris software (version 7.4.2), the ratio between live cells and dead cells was calculated using the green and red fluorescence intensity data (Robertson et al., 2019).

2.4. Microbial community analysis.

The total microbial DNA was extracted from the biofilm using a FastDNA Spin Kit for Soil (Qiagen, CA, USA). The bacterial 16S rRNA genes at V4-V5 hypervariable regions were amplified with PCR primers 388F (ACTCCTACGGGAGGC AGCAG)) and 806R (GGACTACHVGGGTWTCTAAT). The purification of amplicon DNA was conducted by Majorbio (Shanghai, China) on the Illumina MiSeq platform. The raw sequencing data were uploaded at NCBI Sequence Read Archive with an accession number PRJNA755479. The obtained sequence data were pretreated and analyzed as previously described (Wang et al., 2020b). After filtering the low-quality and chimeric sequences, the high-quality sequences were clustered into operational taxonomic units (OTUs) through UPARSE (version 7.1 http://drive5.com/uparse/) with a 0.03 distance limit (97% similarity level). The sequence taxonomies were generated by an RDP Classifier referring to

211 SILVA (Release132 http://www.arb-silva.de) 16S rRNA database. Alpha diversity and
212 the rarefaction curves were conducted using Mothur software (version v.1.30.1) at a
213 0.97 similarity level.

214 **2.5. Quantification of functional genes and electron transfer mechanism.**

215 The electron transfer-related genes were quantified in triplicate through a real-
216 time quantitative PCR detecting system (ABI 7500, Applied Biosystems, USA)
217 including *pil*A, and *mtr*C (He et al., 2021; Zakaria and Dhar, 2020). The primers of
218 these genes were listed in Table S1. Electron transfer relevant enzymes, including
219 cytochrome c (extracellular) and NADH (intracellular), were extracted and measured
220 based on volatile suspended solids (VSS) following the previous procedure (Zhang et
221 al., 2021a).

222 **2.6. Statistical analysis.**

223 All data were represented as mean ± SEM (standard error of the mean). Partial
224 least squares discriminant analysis (PLS-DA) was performed between MFCs and
225 MECs using the R package 'mixOmics' (version 3.3.1). Circos was visualized through
226 Circos software (http://circos.ca/). The co-network analysis was drawn using Gephi
227 based on the spearman correlations data output from the R "psych" package. The *p*-
228 value < 0.05 was regarded as statistically significant.

229 **3. Results and discussion**

230 **3.1. Electrochemical response of exoelectrogenic biofilm to PE-MP.**

231 The performance of electrogenesis biofilm under different PE-MP concentrations
232 was investigated in terms of current density output and COD removal efficiency in
233 MFCs and MECs. Fig. 1a shows that different PE-MP concentrations did not
234 significantly influence the current density output from MFCs. However, in the MECs
235 mode, the maximum current density decreased with the increase of PE-MP

236 concentration (1.99, 1.37, and 0.74 A/m^2 at 0, 25, and 75 mg/L, respectively) (Fig.
237 1b). In the MFCs, the current was generated from the acetate oxidation by the mature
238 biofilm (Zhang et al., 2011). In this case, the PE-MP might influence only a part of
239 mature biofilm, which was not sufficient to affect the current response. While in the
240 MECs, the current was influenced by the internal resistance at a given applied voltage
241 (Cario et al., 2019). Thus, the decreased current would result from the increased
242 internal resistance in the presence of PE-MP. This result was consistent with the
243 previous study, which reported the decreased volumetric current density with the
244 exposure of silver nanoparticles in MECs (Zakaria and Dhar, 2020).At the end of the
245 batch run, the COD removal efficiency of MFCs with PE-MP was 57.65 ± 8.04 %
246 (MFC75) and 61.93 ± 10.25 % (MFC25) which was lower than that without PE-MP
247 exposure (63.22 ± 0.77 %, MFC0) (Fig. S1a). Similar trends were observed in MECs
248 (Fig. S1b). The COD removal efficiency corresponded with the activity of
249 electrogenesis biofilm, which PE-MP is likely to influence. Fig. S2a and Fig. S2b
250 showed no significant oxidation/reduction peaks during forward and reverse scans.
251 However, the reactor without PE-MP showed higher current generation than that with
252 PE-MP exposure in both MFCs and MECs.

253 EIS was performed to measure the impedance of MESs through the Nyquist plot of
254 the anode electrode. The electrode potential loss mainly include ohmic loss, activated
255 loss, and mass transfer loss, which represent the Rs, Rct, and Rd, respectively The
256 Nyquist plots are shown in Fig. 1c. The total resistance, calculated from the
257 equivalent circuit model, increased from 8.33 Ω in MFC0 to 301.33 Ω in MFC25 and
258 from 35.47 Ω in MEC0 to 91.46 Ω in MEC75. It is clear that the resistance of Rct
259 contributed most of the total resistance, and the resistance increased under the
260 influence of PE-MP. This demonstrated the mass transfer was down with a lower

electron transfer capability (Ren et al., 2019). The toxic of PE-MP might also inhibit some bacteria and increase the mass transfer resistance. Previous research showed that the metal anode deposited nanoparticles can decrease the charge transfer resistances by improving the conductivity of the electrode (Wang et al., 2019). However, in this study, the presence of non-conductive PE-MP increased the Rct from 6.42 Ω (MFC0) to 79.97 Ω (MFC75), and from 28.48 Ω to 83.81 Ω in MEC0 and MEC75. Besides, the toxic of the PE-MP might increase the population of dead cells, resulting in increasing of the electron transfer distance and the charge transfer resistance (Wang et al., 2020a). The results might be ascribed to the influence of PE-MP on the activity and viability of the electrogenic biofilm and the weakened EET process. In the future studies, catalyst-free cathode could be employed to reduce the capital costs for the treatment (Alvarez-Gallego et al., 2012; Pasupuleti et al., 2016). Overall, the multiplexed conductive pathway could be weakened by PE-MP in MESs.

Fig. 1 is here

3.2. Effect of PE-MP on biofilm viability.

The viability of the anodic biofilm under different PE-MP levels was investigated through CLSM imaging. Fig. 2a-c and Fig. 2d-f represent the CLSM z-stack images for MFCs and MECs, respectively. Results showed that a low concentration of MP (25 mg/L) promoted the biofilm viability in MFCs. But when the MPs concentration increased to 75 mg/L, the biofilm viability decreased significantly. To further assess the distribution of dead and live cells, the fluorescence intensity and ratio between live and dead cells based on fluorescence intensity were calculated (Fig. 2g and Fig. 2h). In MFCs the live and dead cells fluorescence intensity all increased at a 25 mg/L PE-MP, and then decreased in higher concentration of PE-MP. However, there was a clear decline of the ratio between live and dead cell with PE-MP concentration

increased from 0 to 75 mg/L (Fig. 2h), with the ratio of dead cells increased from 31.66 ± 1.24 % to 49.72 ± 0.34 %. Low concentration of PE-MP promoted the growth of biofilm bacteria, which was consistent with previous report that the MPs derived nutrients contributed to bacterial growth (Chen et al., 2021). The reduction of live cells fluorescence intensity and ratio of live cells was observed when the concentration of PE-MP increased in MECs. The occurrence of PE-MP could hinder the growth of biofilm in MECs and result in a higher ratio of dead cells, increasing from 37.50 ± 0.65 % to 49.15 ± 3.22 % with PE-MP concentration increased from 0 to 75 mg/L. High MPs will be more harmful to microbiology activities, result in cell dysfunction and inhibit the growth of some functional bacteria. Previous studies have unraveled that polyethylene terephthalate MPs and polyvinyl chloride MPs posed toxicity to the viability of the cell via toxic leachate from microplastics, which would result in cell death (Wei et al., 2021; Zhang et al., 2020a). It has also been reported that the MPs in marine could cause negative effects on the organism (Sun et al., 2018). Same with our study, the growth of exoelectrogenic microbes and their attachment to the electrode was inhibited at higher MPs concentration because of the toxicities (agree with the overlay CLSM, Fig. S3). The presence of more dead cells might affect the EET process since the electron product from the live cells had to transfer over the dead cells to the electrode (Sun et al., 2015). The death cells layer could increase the electrode resistance, which was also shown from the EIS result that the relative higher dead cells resulted in a relative high resistant (Liang et al., 2011). The MFC75 showed relatively lower dead cells, and thus, the internal resistance was relatively lower than that of MFC25.

Fig. 2 is here

3.3. EPS distribution in the exoelectrogenic biofilm.

311 The abundance of EPS could reveal the performance of anodic biofilm (Li et al.,
312 2021). Thus, fluorescence spectroscopy was used to fingerprint LB_EPS and TB_EPS
313 in the processed EPS samples (Fig. S4 and Fig. 3). Optical fingerprints distinguished
314 between the different EPS fractions and experimental treatments (Fig. S5). It has been
315 well-documented that the difference among various types of EPS resulted from the
316 functional particular components distribution (Li et al., 2021). The lightly bound EPS
317 can easily be loose under the influence of the PE-MP, and the TB_EPS was more
318 stably attached to the exoelectrogenic bacteria (He et al., 2019). This is the reason
319 why they clustered differently.

320 As shown in Fig. 3a-f, two main peaks Peak T and Peak C were observed at
321 Ex/Em of 275/330 nm and 337/447 nm, which was assumed to be a proxy for protein-
322 like and humic-like fractions (Li et al., 2016; Wei et al., 2016). The normalized FI of
323 each peak was summarized to examine qualitative variation of the substrates. The FI
324 of Peak T for TB_EPS was reduced with different doses of MPs in MFCs. A similar
325 result was observed for MECs, except for a slight increase when it varied from
326 MEC25 (0.77 ± 0.29) to MEC75 (1.09 ± 0.34) (Fig. 3a-f, and Fig. S4g). Previous
327 observation of protein production in EPS showed that protein could be promoted
328 under microbial electrochemical cultivation process or the suitable anode potential,
329 and was likely being involved in the EET process (Hou et al., 2020; Li et al., 2021).
330 The distinct suppression in the EPS protein has also been previously demonstrated in
331 anaerobic methane recovery experiment with polyvinyl chloride MPs exposure
332 (Zhang et al., 2020a). Here, PE-MP might inhibit the protein production in the
333 electroactive bacteria and thereby weakening the EET process in MESs. Also the
334 decreasing of the EPS under the influence of PE-MP could expose the bacteria to the
335 outside toxic chemicals resulting in cells death and thereby weakening the

336 performance of the electroactive bacteria. Similarly, more markedly reduced Peak T
337 could be observed for LB_EPS (Fig. S4a-f). As the lightly bound EPS, the LB_EPS
338 was more easily influenced with the exposure of PE-MP.

339 Humic substances have been well known as the electron mediators involved in
340 the indirect EET pathway, and it can also shift the community structure (Xiao and
341 Zhao, 2017). It seems no compositional changes in the area of Peak C (humic-like
342 substrates) according to the fluorescence in MFCs (Fig. 3a-c, and Fig. S4h). Thus, the
343 PE-MP seems did not play a critical role in changing the content of humic-like
344 substrates in MFCs. Comparatively, PE-MP affected the humic-like substrate in
345 MECs (Fig. 3d-f , Fig. S4h). The Peak C with the highest in LB_EPS in MECs (Fig.
346 S4d-f).

347 Thus, MPs might first affect the protein and humic-like substrates composition in EPS
348 which as demonstrated as an important substance for the electrochemical activity of
349 the biofilm in MESs (Xiao and Zhao, 2017). Furthermore, the exposed bacteria might
350 be inhibited by the toxic compounds from the PE-MP, which would also be the reason
351 for the increased dead cells ratio when PE-MP existed. Detailed mechanism analysis
352 are required in future studies to reveal the synergistic interactions among MPs, EPS
353 and electroactive biofilm.

354 Fig. 3 is here

355 **3.4. The effect of MPs on the microbial community of exoelectrognic biofim**.

356 A total of 420 OTUs identified from all the samples with a 97% sequence
357 similarity. Rarefaction curves showed that the microbial richness exposure to PE-MP
358 decreased compared to the control (Fig. 4a). Similarly, decrease in richness was found
359 through Chao 1 and Ace estimator (Table 1). The richness of bacterial communities on
360 PE-MP has also been reported lower than that in natural substrates (Miao et al., 2019).

The presence of microplastics would be toxic to the cell growth, which could also be reflected by the decreased cell viability and EPS. Microbial diversity Shannon estimator increased in MFCs with PE-MP from 2.198 (MFC0) to 2.759 (MFC25) and 2.550 (MFC75) but declined in MECs (Table 1), indicating that some microbial communities are sensitive to the PE-MP toxic effects (Zhang and Chen, 2020). In addition, PLS-DA was conducted to evaluate the microbial community structure alterations and reveal whether there are differences among different group samples. A clear difference between MFCs and MECs were existed, indicating the varied community structures under different modes (Fig. 4b). Significant cluster for MEC25 and MEC75 showing the species selectivity from PE-MP in MECs. Previous research has also demonstrated the obvious different microbial communities between plastic and non-plastic substrates (Miao et al., 2019).

The identified OTUs were assigned to 21 phyla, 293 genus, and 361 species. The composition of phylum among these six samples was presented in Fig. 4c using Circos. The five most abundant phyla were Proteobacteria, Bacteroidota, Actinobacteriota, Firmicutes, and Desulfobacterota. As the most abundant phyla, Proteobacteria showed an increasing trend in MFCs with the PE-MP concentrations increase. Specifically, it increased from 63.21% in MEC0 to 78.50% (MEC25) and 85.42% (MEC75). The relative abundance of Firmicutes also increased with the PE-MP in both MFCs (5.13% to 6.26%) and MECs (5.21% to 7.13%). However significant decrease could be found in MECs for phyla Actinobacteriota, decreasing from 13.82 % in MEC0 to 11.87% in MEC25 and 1.76% in MEC75.

The 50 most abundant genera from the microbial communities of six samples were shown as heatmap in Fig. S6. The several high abundant genera are widely found in MESs, such as *Acinetobacter*, Bacteroidales (no rank at genus level),

386 *Dechlorosoma*, and *Desulfovibrio* (Wang et al., 2020a; Zakaria and Dhar, 2020;
387 Zhang et al., 2021b). Functional genera of EAB were selected and visualized using a
388 heatmap (Fig. 4d). As one of the most famous EAB, *Geobacter* could oxidize acetate
389 and release electricity in MESs (Kimura and Okabe, 2013). In the MECs, the
390 abundance of *Geobacter* decreased from 6.49% (MEC0) to 0.71% (MEC25) and
391 0.05% (MEC75) with increasing of the PE-MP concentration. However, in MFCs, the
392 abundance increased slightly in MFC25, and then it decreased to the same level as
393 MFC0 and MFC75. *Mycobacterium* was also weakened in MEC25 (1.38%) and
394 MEC75 (0.12%) compared with that without PE-MP (8.03%) in MEC0. It has been
395 reported that M*ycobacterium* has the ability of EET (Jin et al., 2018). A decreased
396 trend could also be found in MECs for genus *Comamonas* that is capable of electron
397 transfer (Yang et al., 2019). With the increasing of PE-MP concentration, *Romboutsia*,
398 which was reported as potential electricigens in soil MFCs (Li et al., 2018), decreased
399 not only in MECs (0.96% to 0.32%) but also in MFCs (0.62% to 0.08%). Besides, the
400 bioelectricity generation related genus *Clostridium_sensu_stricto_13* and
401 *Dysgonomonas* in MFCs shrank with PE-MP (Li et al., 2018; Tian et al., 2017). When
402 comparison of the abundance in all MFCs, it was observed that some genera in
403 MFC25 had a higher abundance than MFC0 and also MFC75, which include
404 *Geobacter*, *Desulfovibrio*, *Clostridium_sensu_stricto_1*, *Parabacteroides*, *Bacillus*,
405 and *Pseudomonas*. The results indicated that the low-level PE-MP might motivate the
406 growth of some electrogenic bacteria. This phenomenon could also be reflected in the
407 CV curve and the CLSM analysis (Fig. S2a, and Fig. 2b). Among all the functional
408 genus, *Bacillus* was the only one who was reported that could generate electricity and
409 degrade polyethylene plastics (Auta et al., 2017; Islam et al., 2017). So the low
410 concentration of PE-MP might serve as the substrate and increase the growth of

411 *Bacillus,* while the high concentration might have toxicity to the cell. The above
412 results demonstrated that the presence of PE-MP could alter the anodic microbial
413 communities, esspecially the ones are known for EET.

414 Table 1. is here

415 Fig. 4 is here

416 It is still not clear about the distribution pattern of EAB and the interaction
417 between PE-MPs concentrations and all the biofilm community. Thus, co-occurrence
418 network analyses were constructed among PE-MP concentrations (marked as MPs),
419 the summary abundance of the exoelectrogenic bacteria (marked as EAB here), and
420 the abundance of all OTUs from different modes of samples. The EAB was
421 summarized as one consortium to easily evaluate the relationship between EAB as a
422 total community and the individual OTUs. In MFCs, the interaction of total EAB
423 abundance, PE-MP concentrations, and 314 OTUs was visualized in Fig. 5a, showing
424 significant Spearman correlations ($p < 0.05$). Among all the OTUs nodes, 86 nodes
425 with 85 pairs of edges were identified significantly response to the abundance of EAB
426 and PE-MP concentrations. Notably, 38 OUTs showed negative correlations with PE-
427 MP concentrations (38 red edges), higher than that between EAB and OTUs (14 red
428 edges). The positive relationships were less than those two, indicating that the PE-MP
429 concentrations and EAB consortium have a more negative influence on the correlated
430 OTUs in MFCs. There are 109 OTUs nodes and 213 significant correlations between
431 EAB, MPs, and OTUs in the network of MECs (Fig. 5b). Most of the correlations
432 related to PE-MP were negative (82 red edges), while most of the EAB-related
433 relationships were positive (81 blue edges). These observations suggested that PE-MP
434 concentrations had a remarkable negative effect on the microbial taxon in MFCs and
435 MECs. This showed that the toxic effect of PE-MP on the EAM growth. It has been

436 previously reported that the polyvinyl chloride MPs could negatively influence the
437 content of some key acidogens and methanogens in anaerobic digestion systems
438 (Zhang et al., 2020a). This was consistent with the observation of the low CLSM
439 intensity in MFC75 and MEC75 (Fig. 2c, and 2f), and low richness reflected by
440 Rarefaction curves (Fig. 4a).

441 Fig. 5 is here

442 **3.5. Quantification of functional genes and EET mechanisms**.

443 In MESs, the current generation is determined by the EET capability of the
444 anodic microbial communities (Wang and Ren, 2013). The effect of MPs on the
445 exoelectrogenic biofilm could be reflected through the transform of the EET pathway.
446 Thus, the expression level of two essential genes related to EET process was
447 evaluated, including *pil*A and *mtr*C (He et al., 2021; Zakaria and Dhar, 2020).
448 Quantitative PCR results revealed that the abundance and expression levels of these
449 two functional genes appeared higher in the samples without PE-MP (MFC0 and
450 MEC0). MEC75 harbored the lowest abundance of the *pli*A gene, while it was similar
451 between MEC0 and MEC25. There was a decline trend of the *mtr*C gene expression
452 with the PE-MP concentrations increased from 0 to 75 mg/L in MFCs (from 1.87 ±
453 0.01 to 1.75 ± 0.01 log(copies/ng DNA)) and MECs (from 1.99 ± 0.03 to 1.68 ± 0.03
454 log(copies/ng DNA)). When the exoelectrogenic biofilm was exposed to the PE-MP,
455 the expression of the EET related genes was inhibited, which down the electron
456 transfer enzymes. The reduced gene expression with MPs exposure would result from
457 the low percentage of EAB according to Fig. 4d.

458 As the membrane-bound redox protein, cytochrome c plays a key role in EET
459 process (Xiao and Zhao, 2017). In the MFCs, the highest abundant cytochrome c was
460 found in MFC25 (5.18 ± 1.03 mg/g VSS), while MFC75 (2.77 ± 0.62 mg/g VSS) has

the lowest level. The resulst imply that the low concentration of PE-MP could accelerate the EET while the high content of PE-MP would inhibit it. The CLSM and EAB abundance analysis also confirmed the rich bacteria grow on the surface of the anode in MFC25 (Fig. 2a and Fig. 4d). In contrast, cytochrome c content in MECs sharply dropped with the presence of PE-MP, similar as the circuit current shown in Fig. 1b. The gene encoded cytochrome c could be the electron shuttle, assisting the transfer of electrons. Meanwhile, cytochrome c-containing subunit II was reported to decrease with polyethersulfone MPs addition in the nitrifying process (Qin et al., 2020). Thus, the drop of cytochrome c in exoelectrogenic biofilm may result from the low expression of electrogenic genes and the abundance of EAB. In the previous case, c-type cytochrome expression could be influenced under intermittent electro-driving electrochemical biofilms (Wang et al., 2020a). It hinted at the different results in different MESs. As the intracellular electron carrier, NADH was facilitated in the MFCs with the occurrence of PE-MP, while it was repressed in MECs (Fig. 6b). Although electrons could be transported through NADH dehydrogenase, it is difficult to identify the influence of PE-MP on NADH in other MESs (Rabaey and Verstraete, 2005). In this study, we could elucidate that the electron carriers were upregulated with PE-MP in MFCs, but it turned to the opposite in MECs.

Fig. 6 is here

4. Conclusions

In this study, the influence of PE-MP on the electrogenic bacteria in MFCs and MECs was demonstrated for the first time. It was found that the current density showed no significate difference with the occurrence of PE-MP in MFCs, but decreased with the increase of PE-MP concentration in MECs. Besides, the presence of PE-MP decreased the COD removal efficiency, while it increased the resistance of

anode biofilm in both systems. A low concentration of PE-MPs could enhance exoelectrogens viability in MFCs, but the high content of PE-MP may suppress the viability in both MFCs and MECs. In addition, the ratio of the dead cell increased from 31.66 ± 1.24 % to 49.72 ± 0.34 % in the MFCs and from 37.50 ± 0.65 % to 49.15 ± 3.22 % in the MECs, reflecting a toxic effect of MPs on the exoelectrogens biofilm. The presence of PE-MPs decreased the protein content in EPS. Moreover, the richness of the microbial communities in the biofilm decreased with the increase of PE-MP level. EAB abundance increased after adding 25 mg/L MPs in MFCs, but it dropped with PE-MP in MECs. Furthermore, most of the MP-related OTUs were significantly negative with PE-MP according to co-network. The effect of microplastics on EET-related genes and membrane-bound cytochrome c was evaluated for the first time in this study. The reduction of the EET would decrease the efficiency of the microbial electrochemical processes. This is the first study revealing the role of microplastics in the microbial electrochemical systems treating wastewater. The results will address an intriguing question in science, add to knowledge on environmental impact of microplastics, provide new knowledge for researchers to steer and shape the microbial community to resistant the microplastics toxicity for efficient EET and conductive biofilm development when treating wastewater rich in microplastics. This knowledge will open new opportunities for improving microbial electrochemical processes and developing viable applications for water treatment.

Acknowledgements

The authors would like to acknowledge the China Scholarship Council for the financial support. Yifeng Zhang thanks The Carlsberg Foundation for awarding The Carlsberg Foundation Distinguished Fellowships (CF18-0084).

Declaration of interests

☒ **The authors declare that they have no known competing financial interests or personal relationships that could have appeared to influence the work reported in this paper.**

References

Alvarez-Gallego, Y., Dominguez-Benetton, X., Pant, D., Diels, L., Vanbroekhoven, K., Genné, I. and Vermeiren, P., 2012. Development of gas diffusion electrodes for cogeneration of chemicals and electricity. Electrochim. Acta 82, 415-426.

Association, A.P.H., Association, A.W.W., Federation, W.P.C. and Federation, W.E., 2017 Standard methods for the examination of water and wastewater, American Public Health Association.

Auta, H.S., Emenike, C.U. and Fauziah, S.H., 2017. Screening of Bacillus strains isolated from mangrove ecosystems in Peninsular Malaysia for microplastic degradation. Environ. Pollut. 231(Pt 2), 1552-1559.

Avio, C.G., Gorbi, S. and Regoli, F., 2017. Plastics and microplastics in the oceans: From emerging pollutants to emerged threat. Mar. Environ. Res. 128, 2-11.

Bajracharya, S., Sharma, M., Mohanakrishna, G., Dominguez Benneton, X., Strik, D.P.B.T.B., Sarma, P.M. and Pant, D., 2016. An overview on emerging bioelectrochemical systems (BESs): Technology for sustainable electricity, waste remediation, resource recovery, chemical production and beyond. Renew. Energy 98, 153-170.

Berezina, N.P., Kononenko, N.A., Dyomina, O.A. and Gnusin, N.P., 2008. Characterization of ion-exchange membrane materials: properties vs structure. Adv. Colloid Interface Sci. 139(1-2), 3-28.

Cario, B.P., Rossi, R., Kim, K.Y. and Logan, B.E., 2019. Applying the electrode potential slope method as a tool to quantitatively evaluate the performance of individual microbial electrolysis cell components. Bioresour. Technol. 287, 121418.

Chen, X., Wang, Y., Chen, S., Sun, Y., Tan, Q., Ding, Z., Lu, Y. and Yu, Y., 2021. Microplastics as carbon-nutrient sources and shaper for microbial communities in stagnant water. J. Hazard. Mater. 420, 126662.

Chiranjeevi, P. and Patil, S.A., 2020. Strategies for improving the electroactivity and specific metabolic functionality of microorganisms for various microbial electrochemical technologies. Biotechnol. Adv. 39, 107468.

Coble, P.G., 2007. Marine optical biogeochemistry: the chemistry of ocean color. Chem. Rev. 107(2), 402-418.

Cole, M. and Galloway, T.S., 2015. Ingestion of Nanoplastics and Microplastics by Pacific

548 Oyster Larvae. Environ. Sci. Technol. 49(24), 14625-14632.
549 Cook, S., Chan, H.L., Abolfathi, S., Bending, G.D., Schafer, H. and Pearson, J.M., 2020.
550 Longitudinal dispersion of microplastics in aquatic flows using fluorometric
551 techniques. Water Res. 170, 115337.
552 Fu, S., Angelidaki, I. and Zhang, Y., 2021. *In situ* Biogas Upgrading by CO2-to-CH4
553 Bioconversion. Trends Biotechnol. 39(4), 336-347.
554 He, P., Zhou, Y., Shao, L., Huang, J., Yang, Z. and Lu, F., 2019. The discrepant mobility of
555 antibiotic resistant genes: Evidence from their spatial distribution in sewage sludge
556 flocs. Sci. Total. Environ. 697, 134176.
557 He, C., Zhang, B., Lu, J. and Qiu, R., 2021. A newly discovered function of nitrate reductase
558 in chemoautotrophic vanadate transformation by natural mackinawite in aquifer.
559 Water Res. 189, 116664.
560 Hidayaturrahman, H. and Lee, T.G., 2019. A study on characteristics of microplastic in
561 wastewater of South Korea: Identification, quantification, and fate of microplastics
562 during treatment process. Mar. Pollut. Bull. 146, 696-702.
563 Hou, R., Luo, C., Zhou, S., Wang, Y., Yuan, Y. and Zhou, S., 2020. Anode potential-dependent
564 protection of electroactive biofilms against metal ion shock via regulating
565 extracellular polymeric substances. Water Res. 178, 115845.
566 Islam, M.A., Ethiraj, B., Cheng, C.K., Yousuf, A. and Khan, M.M.R., 2017. Electrogenic and
567 Antimethanogenic Properties of Bacillus cereus for Enhanced Power Generation in
568 Anaerobic Sludge-Driven Microbial Fuel Cells. Energ. Fuel. 31(6), 6132-6139.
569 Jin, X., Guo, F., Liu, Z., Liu, Y. and Liu, H., 2018. Enhancing the Electricity Generation and
570 Nitrate Removal of Microbial Fuel Cells With a Novel Denitrifying Exoelectrogenic
571 Strain EB-1. Front. Microbiol. 9, 2633.
572 Karygianni, L., Ren, Z., Koo, H. and Thurnheer, T., 2020. Biofilm Matrixome: Extracellular
573 Components in Structured Microbial Communities. Trends. Microbiol. 28(8), 668-
574 681.
575 Kimura, Z. and Okabe, S., 2013. Acetate oxidation by syntrophic association between
576 Geobacter sulfurreducens and a hydrogen-utilizing exoelectrogen. ISME J. 7(8),
577 1472-1482.
578 Kothawala, D.N., Murphy, K.R., Stedmon, C.A., Weyhenmeyer, G.A. and Tranvik, L.J., 2013.
579 Inner filter correction of dissolved organic matter fluorescence. Limnol. Oceanogr.-
580 Meth. 11(12), 616-630.
581 Kwak, J.I. and An, Y.-J., 2021. Post COVID-19 pandemic: Biofragmentation and soil
582 ecotoxicological effects of microplastics derived from face masks. J. Hazard. Mater.
583 416, 126169.
584 Li, B., Sun, J., Tang, C., Zhou, J., Wu, X., Jia, H., Wei, P., Zhang, Y. and Yong, X., 2021.
585 Coordinated response of Au-NPs/rGO modified electroactive biofilms under phenolic
586 compounds shock: Comprehensive analysis from architecture, composition, and
587 activity. Water Res. 189, 116589.
588 Li, Y., Li, X., Sun, Y., Zhao, X. and Li, Y., 2018. Cathodic microbial community adaptation to
589 the removal of chlorinated herbicide in soil microbial fuel cells. Environ. Sci. Pollut.
590 R 25(17), 16900-16912.
591 Li, Y., Yuan, X., Wu, Z., Wang, H., Xiao, Z., Wu, Y., Chen, X. and Zeng, G., 2016. Enhancing

the sludge dewaterability by electrolysis/electrocoagulation combined with zero-valent iron activated persulfate process. Chem. Eng. J. 303, 636-645.

Liang, D., Peng, S., Lu, S., Liu, Y., Lan, F. and Xiang, Y., 2011. Enhancement of hydrogen production in a single chamber microbial electrolysis cell through anode arrangement optimization. Bioresource Technol. 102(23), 10881-10885.

Luo, X., Zhang, F., Liu, J., Zhang, X., Huang, X. and Logan, B.E. 2014. Methane production in microbial reverse-electrodialysis methanogenesis cells (MRMCs) using thermolytic solutions. Environ. Sci. Technol. 48(15), 8911-8918.

Miao, L., Wang, P., Hou, J., Yao, Y., Liu, Z., Liu, S. and Li, T., 2019. Distinct community structure and microbial functions of biofilms colonizing microplastics. Sci. Total. Environ. 650(Pt 2), 2395-2402.

Murphy, K.R., Stedmon, C.A., Graeber, D. and Bro, R., 2013. Fluorescence spectroscopy and multi-way techniques. PARAFAC. Anal. Methods. 5(23), 6557.

Niu, L., Li, Y., Li, Y., Hu, Q., Wang, C.D., Hu, J., Zhang, W., Wang, L., Zhang, C. and Zhang, H., 2021. New insights into the vertical distribution and microbial degradation of microplastics in urban river sediments. Water Res. 188, 116449.

Pasupuleti, S.B., Srikanth, S., Dominguez-Benetton, X., Mohan, S.V. and Pant, D., 2016. Dual gas diffusion cathode design for microbial fuel cell (MFC): optimizing the suitable mode of operation in terms of bioelectrochemical and bioelectro-kinetic evaluation. J. Chem. Technol. Biotechnol. 91(3), 624-639.

Peeken, I., Primpke, S., Beyer, B., Gutermann, J., Katlein, C., Krumpen, T., Bergmann, M., Hehemann, L. and Gerdts, G., 2018. Arctic sea ice is an important temporal sink and means of transport for microplastic. Nat. Commun. 9(1), 1505.

Qin, R., Su, C., Liu, W., Tang, L., Li, X., Deng, X., Wang, A. and Chen, Z., 2020. Effects of exposure to polyether sulfone microplastic on the nitrifying process and microbial community structure in aerobic granular sludge. Bioresource Technol. 302, 122827.

Rabaey, K. and Verstraete, W., 2005. Microbial fuel cells: novel biotechnology for energy generation. Trends Biotechnol. 23(6), 291-298.

Ren, G., Chen, P., Yu, J., Liu, J., Ye, J. and Zhou, S., 2019. Recyclable magnetite-enhanced electromethanogenesis for biomethane production from wastewater. Water Res. 166, 115095.

Robertson, J., McGoverin, C., Vanholsbeeck, F. and Swift, S., 2019. Optimisation of the Protocol for the LIVE/DEAD((R)) BacLight(TM) Bacterial Viability Kit for Rapid Determination of Bacterial Load. Front. Microbiol. 10, 801.

Rochman, C.M., 2018. Microplastics research—from sink to source. Science 360(6384), 2.

Sarkar, D.J., Sarkar, S.D., Mukherjee, S. and Das, B.K., 2021 Contaminants in Drinking and Wastewater Sources, pp. 95-115, Springer.

Seeley, M.E., Song, B., Passie, R. and Hale, R.C., 2020. Microplastics affect sedimentary microbial communities and nitrogen cycling. Nat. Commun. 11(1), 2372.

Seidensticker, S., Zarfl, C., Cirpka, O.A., Fellenberg, G. and Grathwohl, P., 2017. Shift in Mass Transfer of Wastewater Contaminants from Microplastics in the Presence of Dissolved Substances. Environ. Sci. Technol. 51(21), 12254-12263.

Sun, D., Cheng, S., Wang, A., Li, F., Logan, B.E. and Cen, K., 2015. Temporal-spatial changes in viabilities and electrochemical properties of anode biofilms. Environ. Sci.

Technol. 49(8), 5227-5235.
Sun, X., Chen, B., Li, Q., Liu, N., Xia, B., Zhu, L. and Qu, K., 2018. Toxicities of polystyrene nano- and microplastics toward marine bacterium Halomonas alkaliphila. Sci. Total. Environ. 642, 1378-1385.
Sun, X., Yuan, X., Jia, Y., Feng, L., Zhu, F., Dong, S., Liu, J., Kong, X., Tian, H., Duan, J., Ding, Z., Wang, S. and Xing, B., 2020. Differentially charged nanoplastics demonstrate distinct accumulation in Arabidopsis thaliana. Nature nanotechnol. 15(9), 755-760.
Tang, Q., Wu, M., Zhang, Y., Li, J., Liang, J., Zhou, H., Qu, Y. and Zhang, X., 2021. Performance and bacterial community profiles of sequencing batch reactors during long-term exposure to polyethylene terephthalate and polyethylene microplastics. Bioresource Technol. https://doi.org/10.1016/j.biortech.2021.126393.
Tian, Y., Mei, X., Liang, Q., Wu, D., Ren, N. and Xing, D., 2017. Biological degradation of potato pulp waste and microbial community structure in microbial fuel cells. RSC Adv. 7(14), 8376-8380.
Trevisan, R., Voy, C., Chen, S. and Di Giulio, R.T., 2019. Nanoplastics decrease the toxicity of a complex PAH mixture but impair mitochondrial energy production in developing zebrafish. Environ. Sci. Technol. 53(14), 8405-8415.
Vollertsen, J. and Hansen, A.A., 2017. Microplastic in Danish wastewater: Sources, occurrences and fate.
Wang, B., Liu, W., Zhang, Y. and Wang, A., 2020a. Bioenergy recovery from wastewater accelerated by solar power: Intermittent electro-driving regulation and capacitive storage in biomass. Water Res. 175, 115696.
Wang, S., Zhang, B., Li, T., Li, Z. and Fu, J., 2020b. Soil vanadium (V)-reducing related bacteria drive community response to vanadium pollution from a smelting plant over multiple gradients. Environ. Int. 138, 105630.
Wang, H. and Ren, Z., 2013. A comprehensive review of microbial electrochemical systems as a platform technology. Biotechnol. Adv. 31(8), 1796-1807.
Wang, W., Zhang, B. and He, Z., 2019. Bioelectrochemical deposition of palladium nanoparticles as catalysts by Shewanella oneidensis MR-1 towards enhanced hydrogen production in microbial electrolysis cells. Electrochim. Acta 318, 794-800.
Wei, D., Li, M., Wang, X., Han, F., Li, L., Guo, J., Ai, L., Fang, L., Liu, L., Du, B. and Wei, Q., 2016. Extracellular polymeric substances for Zn (II) binding during its sorption process onto aerobic granular sludge. J. Hazard. Mater.301, 407-415.
Wei, W., Chen, X., Peng, L., Liu, Y., Bao, T. and Ni, B., 2021. The entering of polyethylene terephthalate microplastics into biological wastewater treatment system affects aerobic sludge digestion differently from their direct entering into sludge treatment system. Water Res. 190, 116731.
Woodward, J., Li, J., Rothwell, J. and Hurley, R., 2021. Acute riverine microplastic contamination due to avoidable releases of untreated wastewater. Nat. Sustain. 4(9), 793-802.
Xiao, Y. and Zhao, F., 2017. Electrochemical roles of extracellular polymeric substances in biofilms. Curr. Opin. Electrochem. 4(1), 206-211.
Xu, M., Zhou, H., Zou, R., Yang, X., Su, Y., Angelidaki, I. and Zhang, Y., 2021. Beyond the

680 farm: Making edible protein from CO2 via hybrid bioinorganic electrosynthesis. One
681 Earth 4(6), 868-878.
682 Yang, J., Cheng, S., Li, P., Huang, H. and Cen, K., 2019. Sensitivity to Oxygen in Microbial
683 Electrochemical Systems Biofilms. iScience 13, 163-172.
684 Yang, X., Zou, R., Tang, K., Andersen, H.R., Angelidaki, I. and Zhang, Y., 2021. Degradation
685 of metoprolol from wastewater in a bio-electro-Fenton system. Sci. Total. Environ.
686 771, 145385.
687 Zakaria, B.S. and Dhar, B.R., 2020. Changes in syntrophic microbial communities, EPS
688 matrix, and gene-expression patterns in biofilm anode in response to silver
689 nanoparticles exposure. Sci. Total. Environ. 734, 139395.
690 Zhang, B., Li, Y., Fei, Y. and Cheng, Y., 2021a. Novel Pathway for Vanadium(V) Bio-
691 Detoxification by Gram-Positive Lactococcus raffinolactis. Environ. Sci. Technol.
692 55(3), 2121-2131.
693 Zhang, Y., Xu, Y., Chen, X., Chen, C., Sun, J., Bai, X. and Yuan, Y., 2021b. Effect of copper
694 ions on glucose fermentation pathways in bioelectrochemical system. Chemosphere
695 272, 129627.
696 Zhang, L., Zhu, X., Li, J., Liao, Q. and Ye, D., 2011. Biofilm formation and electricity
697 generation of a microbial fuel cell started up under different external resistances. J.
698 Power Sources 196(15), 6029-6035.
699 Zhang, Y., Wei, W., Sun, J., Xu, Q. and Ni, B., 2020a. Long-Term Effects of Polyvinyl
700 Chloride Microplastics on Anaerobic Granular Sludge for Recovering Methane from
701 Wastewater. Environ. Sci. Technol. 54(15), 9662-9671.
702 Zhang, Z. and Chen, Y., 2020b. Effects of microplastics on wastewater and sewage sludge
703 treatment and their removal: A review. Chem. Eng. J. 382, 122955.
704 Zhao, N., Treu, L., Angelidaki, I. and Zhang, Y., 2019. Exoelectrogenic Anaerobic Granular
705 Sludge for Simultaneous Electricity Generation and Wastewater Treatment. Environ.
706 Sci. Technol. 53(20), 12130-12140.
707
708
709
710
711

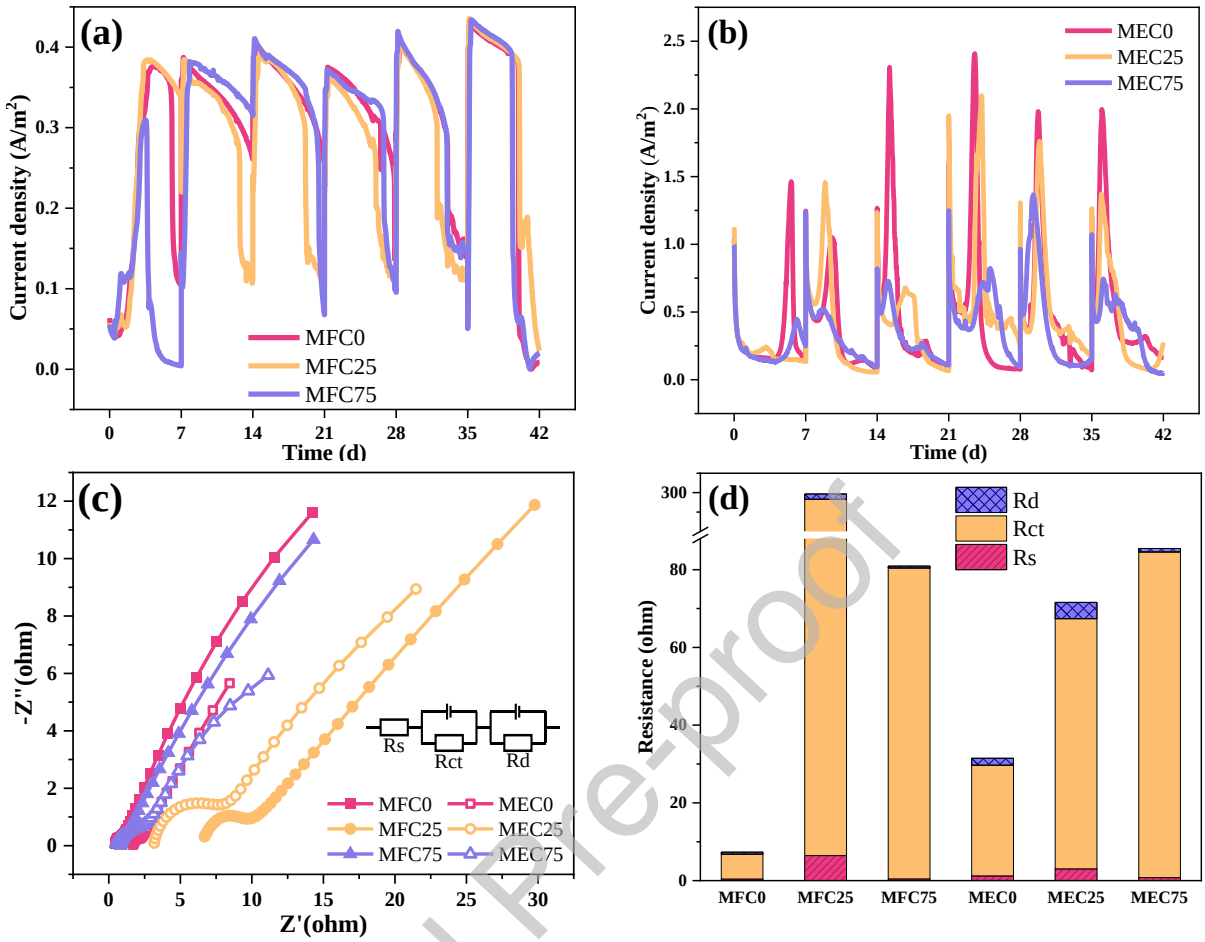

712 Fig. 1 The performance and electrochemical activity of MESs. (a) Current density
713 output in MFCs; (b) Current density response in MECs; (c) and (d) show Nyquist
714 plots and internal resistances analyzed by fitting to the equivalent circuit for the anode
715 biofilm via EIS.

716

717

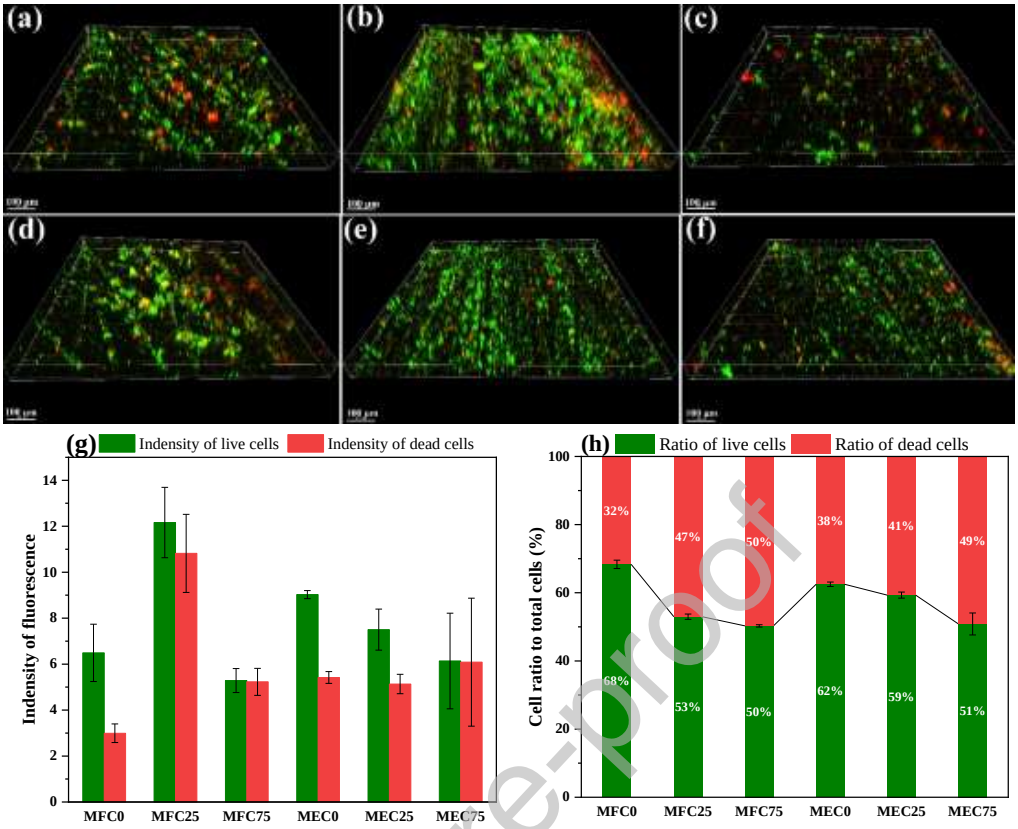

718 Fig. 2 Evaluation of the effect of MPs on anode biofilm matrix structure and
719 quantification by CLSM through staining live and dead cells. The live cells were
720 stained green, and red labeled the dead cells. CLSM images of anode biofilm in MFCs
721 (a, b, c) and MECs (d, e, f) following the concentrations of 0, 25, 75 mg/L; (g) mean
722 fluorescence intensity calculated from three random CLSM data of each sample; (h)
723 ratio of live and dead cells to total cells based on three random fluorescence intensity
724 of each sample.

725

726

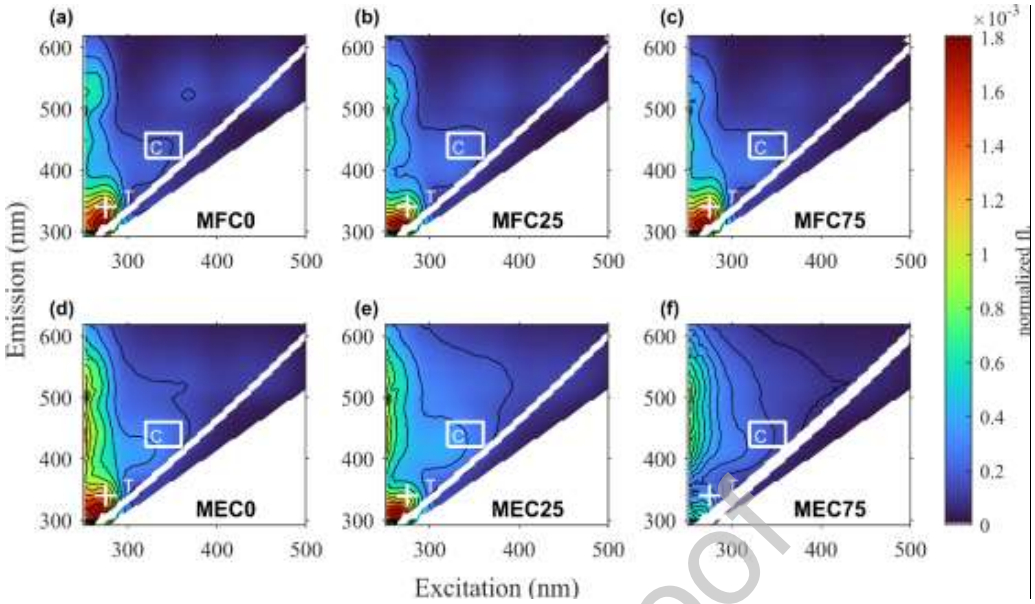

727

728 Fig. 3 EEM fluorescence spectra for the TB_EPS extracted from anode biofilm
729 exposed to different concentration of PE-MP.

730

731

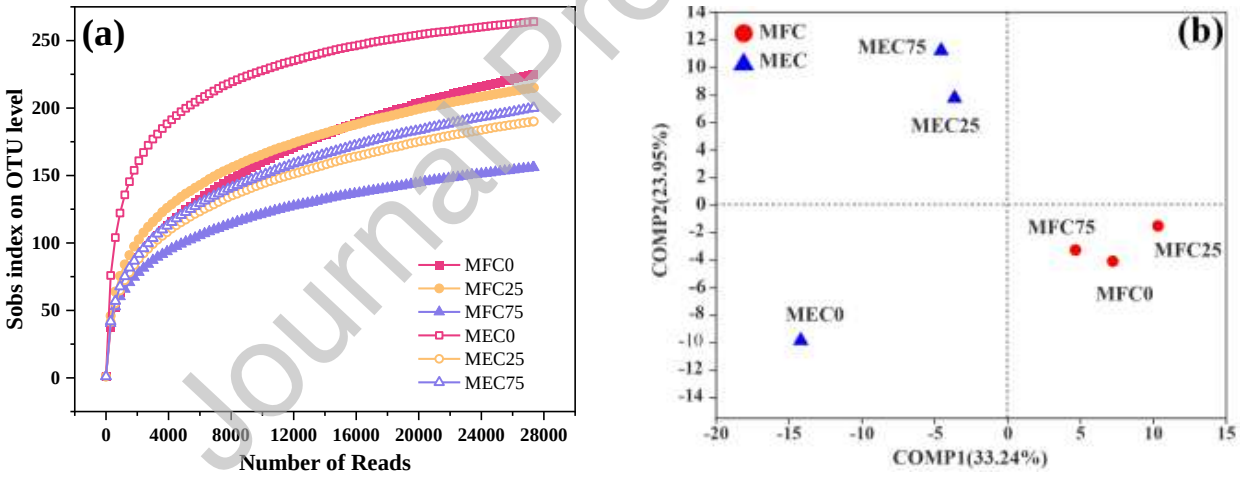

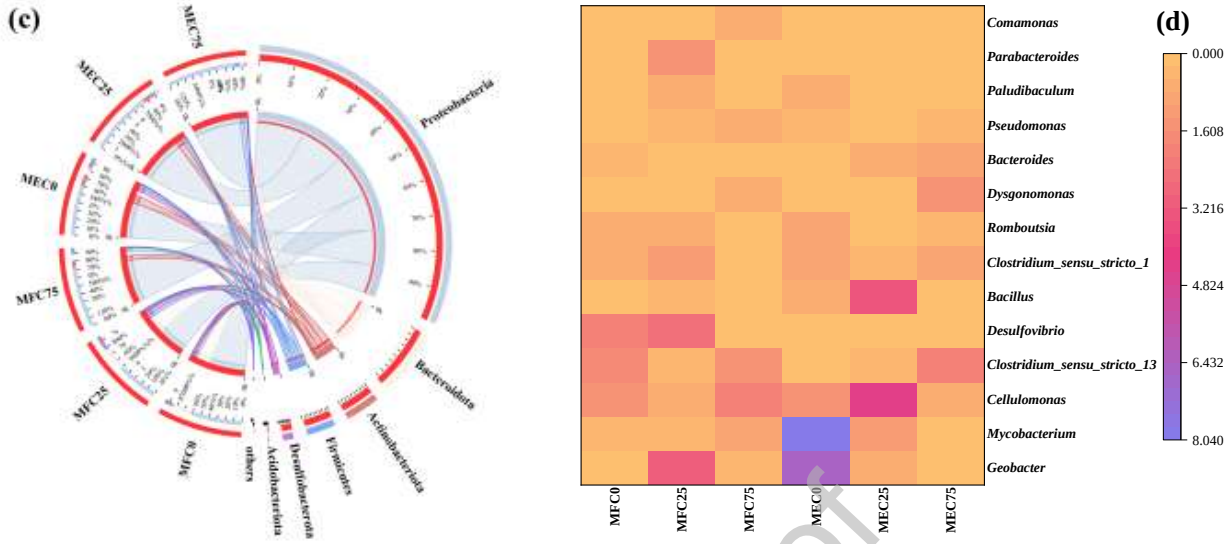

732 Fig. 4 Microbial community constructure and composition for all the samples. (a)
733 Rarefaction curves based on observed Sobs richness; (b) PLS-DA plots; (c) Circos
734 plot of phylum composition; (d) Functional genus composition through heatmap.

735

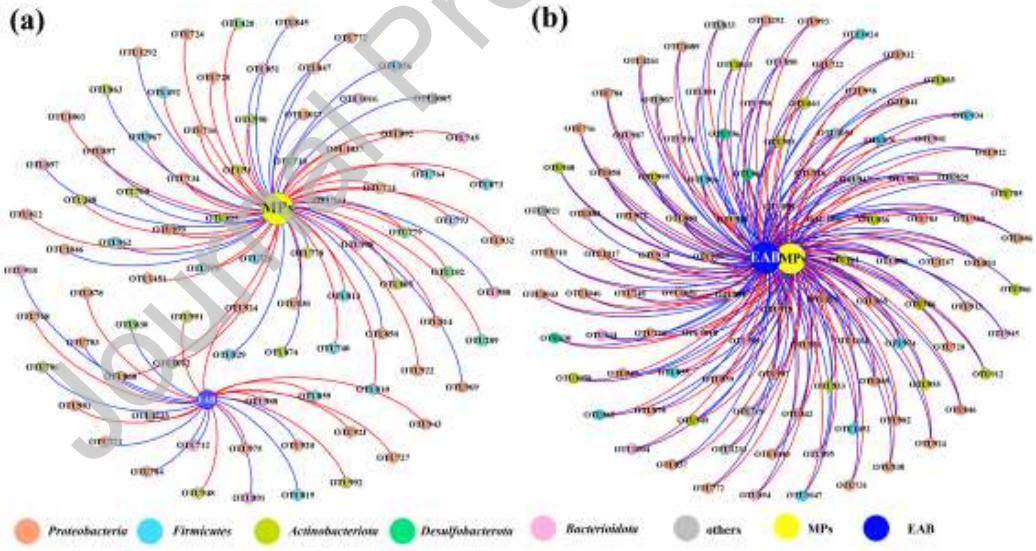

736
737

738 Fig. 5 Co-occurrence network of PE-MP concentration, abundance of EAB, and
739 individual taxa. (a) MFCs; (b) MECs. All the data has been treated by taking log(x+1)
740 value to normalized different data level. Only significant correlations ($p < 0.05$) were
741 visualized. Red line represent negative correlations and the blue lines represent
742 positive correlations. Different color of nodes present different phylum.

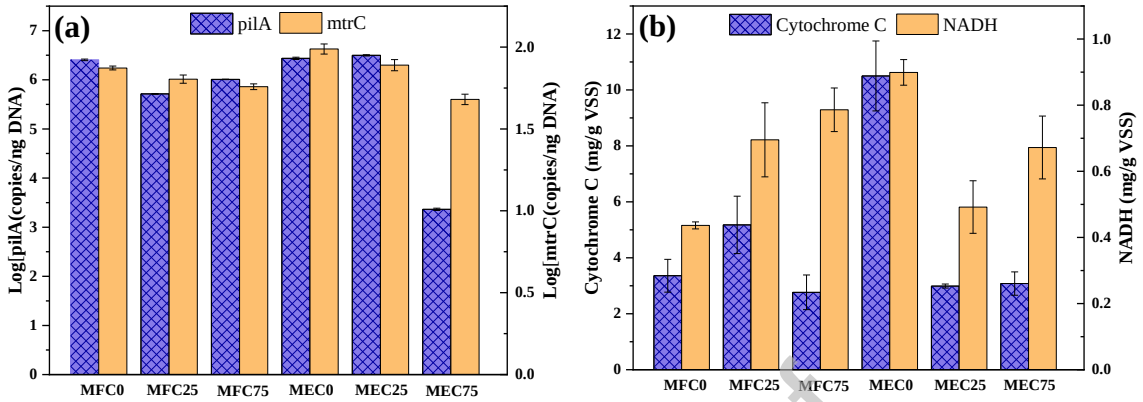

Fig. 6 Quantification and characterization of electron transfer related genes and enzymes. (a) Abundance of *pil*A and *mtr*C genes; (b) Concentrations of cytochrome c and NADH.

Table 1. Alpha-diversity estimator of bacterial communities.

Sample	Sobs	Chao1	Ace	Shannon	Simpson	Coverage
MFC0	225	296.03	302.6672	2.198	0.269316	0.997442
MFC25	215	258.75	265.7764	2.759	0.148716	0.998173
MFC75	156	185.75	192.3035	2.550	0.216605	0.998721
MEC0	264	279.75	281.6843	3.907	0.042937	0.998977
MEC25	190	222.34	236.7272	2.252	0.321146	0.998319
MEC75	200	251.00	254.1899	2.614	0.150836	0.998099